Available online at www.sciencedirect.com
ScienceDirect
Proceedings of the Combustion Institute 32 (2009) 3051–3058
Proceedings of the Combustion Institute
www.elsevier.com/locate/proci

Suppression of combustion instabilities of premixed hydrogen/air flames in microchannels using heterogeneous reactions

Gianmarco Pizza [a,b], John Mantzaras [a,*], Christos E. Frouzakis [b], Ananias G. Tomboulides [c], Konstantinos Boulouchos [b]

[a] *Paul Scherrer Institute, Combustion Research, CH-5232, Villigen PSI, Switzerland*
[b] *Aerothermochemistry and Combustion Systems Laboratory, Swiss Federal Institute of Technology, CH-8092, Zurich, Switzerland*
[c] *Department of Engineering and Management of Energy Resources, University of Western Macedonia, 50100 Kozani, Greece*

Abstract

The dynamics of fuel-lean ($\varphi = 0.5$) premixed hydrogen/air atmospheric pressure flames are investigated numerically in a 1-mm-height planar channel with platinum-coated walls, as a function of the inlet velocity and the catalytic reactivity. Simulations are carried out with a fully elliptic 2D transient code that includes detailed heterogeneous (catalytic) and homogeneous (gas-phase) chemical reaction schemes. The channel wall temperature is prescribed and the inlet properties are uniform, while the catalytic reactivity is controlled by varying the parameter A_s, which is the ratio of the catalytically-active area to the geometrical channel surface area. It is shown that the rich flame dynamics of the non-catalytic case ($A_s = 0$), which include oscillating and asymmetric flame modes, can be suppressed by appropriate selection of the catalytic reactivity. The oscillating flames disappear at $A_s = 6 \times 10^{-3}$ and the asymmetric ones at $A_s = 1.15 \times 10^{-2}$, while for higher values of A_s only stationary and symmetric V-shaped flames are obtained. The suppression of the flame dynamics can be attributed to the theoretically-predicted diminishing sensitivity of the homogeneous ignition distance to small perturbations of the gaseous reactivity with increasing catalytic reactivity. The results indicate that a feasible way to eliminate undesirable unsteady combustion modes in practical microcombustors is to apply a pre-determined catalyst loading on the channel walls.

Keywords: Premixed flame dynamics; Microcombustion; Combustion instabilities; Heterogeneous combustion; Spectral element method

1. Introduction

Combustion at the micro- and meso-scale has attracted increased interest for portable generation of power and heat [1–4]. Channel-flow configurations, in particular, have provided an amenable platform for many experimental and theoretical combustion studies at small scales. Experiments in non-catalytic channels [5–8] have revealed a wealth of combustion dynamics that may pose a concern for the proper operation of

* Corresponding author. Fax: +41 56 310 2199.
E-mail address: ioannis.mantzaras@psi.ch (J. Mantzaras),

1540-7489/$ - see front matter © 2009 The Combustion Institute. Published by Elsevier Inc. All rights reserved.
doi:10.1016/j.proci.2008.05.055

microreactors. Pizza et al. [9] have recently used direct numerical simulation to investigate the stabilization and dynamics of lean premixed hydrogen/air flames in micro-scale planar channels with heights (h) between 0.3 and 1.0 mm, and inlet velocities (U_{IN}) of up to 4 m/s. Therein, a flame stability diagram was constructed in the two-dimensional h–U_{IN} parameter space, clearly delineating all possible flame types and further clarifying many of the earlier experimental observations [5–8]. The richest dynamics were reported for the wider channels [9], starting from periodic ignition/extinction of the flame and further transitioning to symmetric V-shaped flames, asymmetric flames, oscillating flames, and finally again to asymmetric flames as the inlet velocity increased.

Despite the feasibility of pure gas-phase combustion at the microscale, the large surface-to-volume ratios of microreactors call for heterogeneous fuel conversion. Most recent experimental works have thus focused on catalytic channel-flow combustion of hydrocarbon fuels [10–12]. On the numerical front, the stability of catalytic microreactors has so far been addressed only with stationary models. The stability of pure heterogeneous combustion was investigated in a 1-mm gap channel coated with Pt [13]. Recent hetero-/homogeneous studies of CH_4/air combustion over Pt [4] demonstrated the importance of gaseous chemistry in extending the stability limits of catalytic microchannels. It is emphasized that even for the large geometrical confinements typical to catalytic microreactors, gas-phase chemistry cannot always be ignored, particularly at elevated pressures [4,14]. In the specific case of fuel-lean H_2/air mixtures, the onset of homogeneous ignition inside the catalytic reactor is shown to be beneficial since it moderates the superadiabatic surface temperatures attained during the heterogeneous conversion of this diffusionally imbalanced fuel [15]. The dynamics of flames inside catalytic microreactors is thus a topic of practical interest, which has not yet been addressed.

The present work undertakes a numerical investigation of the dynamics of lean ($\varphi = 0.5$) H_2/air flames in catalytic (Pt-coated) microchannels. The main objective is to assess the impact of the catalytic reactions on the gas-phase combustion dynamics. A transient fully elliptic code is used, with detailed hetero-/homogeneous chemistry and transport. The resulting flame dynamics are mapped as a function of two parameters: the inflow velocity, U_{IN}, and the catalytic reactivity, A_s; the latter is controlled by varying the ratio of the active-to-geometrical surface area. Potential implications for the design of microreactors are finally drawn.

2. Computational approach

The configuration consists of a channel flow established between two parallel, infinitely wide plates, with length $L = 10$ mm and height $h = 1$ mm. Details of the numerical method for the non-catalytic channels can be found in [9]. Therefore, a brief model description is provided next with emphasis on the heterogeneous treatment.

2.1. Numerical model

The numerical code solves the transient 2D continuity, momentum, energy, and gas-phase species equations for ideal reactive gases at the low Mach number limit. To account for catalytic chemistry, the surface species coverage (θ_k) equations are additionally solved [16]:

$$\frac{\partial \theta_k}{\partial t} = \frac{\dot{s}_k}{\Gamma} \quad k = 1, \ldots, N_s, \tag{1}$$

with Γ the surface site density of the catalyst, $\dot{s}_k$ the molar catalytic production rate of the kth surface species and N_s the number of surface species.

The gas-phase species interfacial boundary conditions become

$$\vec{n} \cdot \lfloor \rho Y_i (\vec{V}_i + \vec{u}) \rfloor_{wall} = A_s \dot{s}_i W_i \quad i = 1, \ldots, N_g. \tag{2}$$

In Eq. (2), ρ is the gas density, Y_i, $\vec{V}_i$, W_i and $\dot{s}_i$ are the mass fraction, diffusion velocity vector, molecular weight, and molar heterogeneous production rate of the ith gas-phase species, respectively; N_g is the number of gaseous species; $\vec{n}$ is the unit outward-pointing vector normal to the surface, and $\vec{u}$ is the Stefan velocity given by $\vec{n} \cdot \vec{u} = (1/\rho) \sum_{i=1}^{N_g} A_s \dot{s}_i W_i$ [16]. Finally, A_s denotes the ratio of the catalytically active area to the geometrical channel area. A_s is a crucial parameter in the modeling of reactors coated with technical catalysts and can be assessed in practice via CO or H_2 chemisorption experiments [17,18].

A fuel-lean ($\varphi = 0.5$), atmospheric pressure H_2/air premixture is fed at the channel inlet. Uniform inlet velocity (U_{IN}), flux conditions for the incoming species mass fractions and constant inlet temperature ($T_{IN} = 300$ K) are specified at the inflow. The wall temperature is prescribed: over the initial 1/20 channel length, it ramps smoothly via a hyperbolic tangent function from the temperature of the incoming mixture, $T_{IN} = 300$ K, to the final value $T_W = 960$ K. The effects of reaction exothermicity, solid heat conduction, and external heat losses on the true channel wall temperature have been addressed elsewhere [4]. At the channel outlet, zero-Neumann boundary conditions are imposed. For the examined ranges of U_{IN}, the flow is laminar with inlet Reynolds number ranging from 0.5 to 212. Finally, buoyancy is neglected. All the adopted boundary conditions, apart from the species flux condition on the channel walls, are the same with that of the earlier pure homogeneous combustion studies [9], thus isolating the impact of catalytic reactions on the flame dynamics.

For gas-phase chemistry, the elementary mechanism of Kim et al. [19] is employed (9 species and 21 reactions). The detailed surface reaction scheme of Deutschmann et al. [20] (6 gaseous species, 5 surface species and 14 reactions) describes the oxidation of hydrogen on Pt with $\Gamma = 2.7 \times 10^{-9}$ mol/cm^2. A mixture-average transport model is adopted for the species diffusion velocity, while the transport database of CHEMKIN is used [21]. Surface and gas-phase chemical reaction rates are evaluated with CHEMKIN [22] and Surface CHEMKIN [16], respectively.

The parallel code employs the spectral element method for the spatial discretization. The computational domain is split into quadrilateral conforming elements; within each element, Nth order polynomials are used to interpolate the solution in each spatial direction [23]. Time integration is performed with a high-order splitting scheme for low Mach number reactive flows [24], whereby the continuity and momentum equations are integrated with a semi-implicit scheme and the species and energy equations are integrated fully implicitly using the CVODE package [25].

2.2. Computational domain

The entire 2D channel domain (symmetry is not invoked in order to allow for asymmetric solutions) is discretized with eight spectral elements in the transverse direction and 60 elements in the streamwise direction, all equally spaced. To determine the grid requirements, the thermal flame thickness, L_f, is evaluated according to [26]: $L_f = (T_f - T_{IN})/\max|\partial T/\partial x|$, with T_{IN} and T_f the temperatures of the fresh and burned mixture, respectively, and $\max|\partial T/\partial x|$the maximum temperature gradient along the flame coordinate. The flame thickness and laminar flame speed of a freely-propagating lean premixed laminar H_2/air flame ($\varphi = 0.5$, $T_{IN} = 300$ K), computed with the PREMIX code of CHEMKIN [27], are $L_f = 0.39$ mm and $S_L = 58$ cm/s, respectively.

Using sixth-order Legendre–Lagrangian interpolating polynomials per direction and element, a total of 361 axial grid points are used, corresponding to an average spatial resolution of $\Delta x = 0.028$ mm and resulting to approximately $L_f/\Delta x = 14$ grid points within the flame. The solution is not significantly affected by increasing the polynomial order to 8 and subsequently to 10, corresponding to 19 and 23 points inside the flame, respectively, confirming the grid-independence of the solution. Since the grid is even finer in the transverse (y) direction, additional y-resolution tests were not necessary. Simulations were carried out on a Linux cluster with 2.4 GHz CPUs. The stiffness of the surface reactions in Eqs. (1) and (2) resulted in a high computational cost: for a grid consisting of a total of 16,920 discretization points, up to 100 h were necessary on 8 CPUs to obtain a conclusive result for each case investigated, i.e. for each point of the forthcoming Fig. 2. Besides, for the unsteady cases, depending on how fast the solution approaches the limit cycle, up to 100 cycles have been computed. It is noted that full 2D transient simulations (without invoking the quasisteady state assumption for the surface species) have not yet been reported in systems with detailed hetero-/homogeneous reaction schemes.

3. Results and discussion

3.1. Variation of the surface reactivity

The surface reactivity has been varied by adjusting the surface area ratio A_s in Eq. (2). In technical systems with a well-dispersed catalyst, A_s is larger than unity in order to enhance the catalytic conversion rates of the typically less reactive hydrocarbon fuels. In the present studies, however, the very high reactivity of hydrogen on Pt guarantees a mass transport limited catalytic conversion already at $A_s = 1$. Therefore, to investigate the effects of finite-rate surface chemistry on the flame dynamics, A_s has been reduced to sufficiently low values ($3.0 \times 10^{-3} \leqslant A_s \leqslant 1.15 \times 10^{-2}$). In practice, such values can be realized by a very low loading of Pt on the catalyst washcoat (e.g. using the catalyst parameters of [18] and considering a low-limit 0.01% loading of Rh on α-Al_2O_3, corresponding A_s values as low as 4.0×10^{-2} can be obtained).

Figure 1 provides computed axial profiles, considering only catalytic reactions, of the ratio

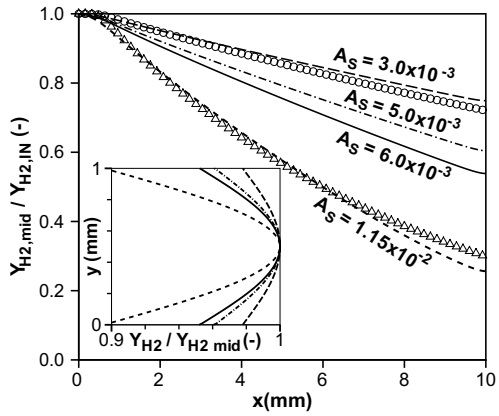

Fig. 1. Hydrogen mass fraction along the mid-plane, $Y_{H_2,mid}$, normalized by the inlet value $Y_{H_2,IN}$: pure catalytic conversion for $U_{IN} = 100$ cm/s at different A_s (the open circles and triangles corresponding to A_s of 3.0×10^{-3} and 1.15×10^{-2}, respectively, were computed using the single step reaction of Section 3.3). The inset provides transverse profiles of Y_{H_2} normalized by the corresponding $Y_{H_2,mid}$, at $x = 5$ mm.

$Y_{H_2,mid}/Y_{H_2,IN}$ for four different A_s, where $Y_{H_2,mid}$ is the hydrogen mass fraction at the channel mid-plane ($y = 0.5$ mm). Even at such low values of A_s, the catalytic fuel depletion is noticeable. On the other hand, the transverse profiles of Y_{H_2} exhibit a moderate variation (less than 10%, see the inset of Fig. 1). It will be shown next that those modest catalytic reactivities are sufficient to drastically alter the underlying flame dynamics.

3.2. Flame dynamics in the presence of catalytic reactions

The flame dynamics under pure gas-phase combustion ($A_s = 0$), are summarized in Fig. 2a (for detailed discussion see [9]). To facilitate the graphical presentation of all flame solutions, a parameter h_{max} has been defined: h_{max} denotes the transverse distance from the lower channel wall ($y = 0$) of the farthest downstream point located at the $Y_{H_2} = 0.007$ iso-level line, non-dimensionalized by the channel height. The following flame types are observed as the inlet velocity increases, Fig. 2a: periodic ignition/extinction, V-shaped flames, asymmetric flames, oscillating flames, and again asymmetric flames that persist for higher U_{IN} until flame blow-out is reached. In the periodic ignition/extinction mode (also observed experimentally in [7]), the flame is characterized by a high frequency repetition (107 Hz at $U_{IN} = 10$ cm/s) of ignition, subsequent upstream propagation and finally extinction close to the channel inlet. The V-shaped flames are steady and symmetric ($h_{max} = 0.5$). The asymmetric flames (attested experimentally in [5]) are also steady, and can either be "upper" or "lower" asymmetric as shown by the Y_{OH} distribution in the insets of Fig. 2. The oscillating flames exhibit a shape which is continuously changing in time (e.g. the frequency is 611 Hz at $U_{IN} = 103.5$ cm/s) between the upper and the lower asymmetric flame solutions (oscillating flames have also been reported in experiments [7]).

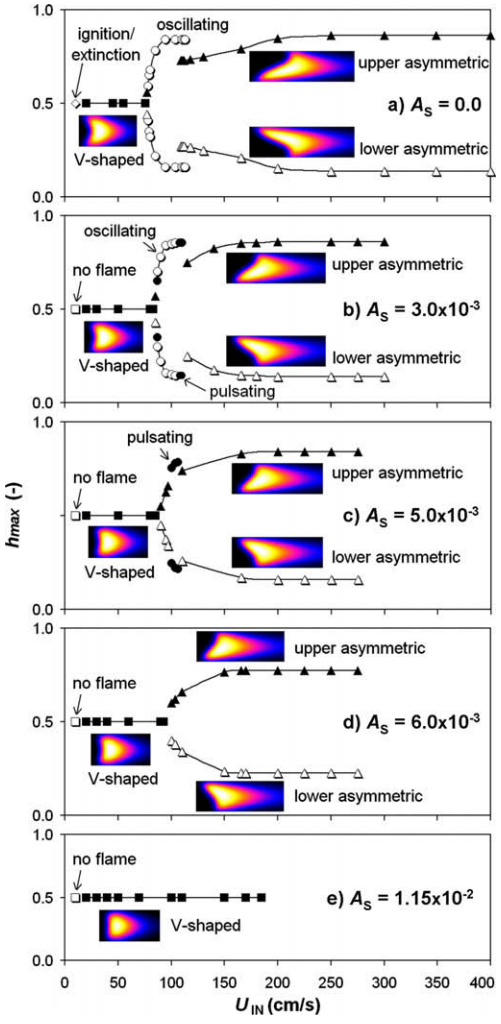

Fig. 2. Flame stability diagram for different surface reactivities: (a) pure homogeneous reactions [9], (b)–(e) gradual suppression of flame instabilities with increasing surface reactivity. The images show the Y_{OH} distributions.

The effect of the catalytic reactivity on the asymmetric flames is analyzed first. Figure 3 illustrates the sequence of shape changes of the originally asymmetric flame at $U_{IN} = 165$ cm/s and $A_s = 0$ (Fig. 3a). As A_s increases, the flame shifts downstream (due to the catalytic depletion of hydrogen), becomes less asymmetric (Fig. 3b and c), and eventually turns to a perfectly symmetric V-shaped flame at $A_s = 1.15 \times 10^{-2}$ (Fig. 3d). For even higher values of A_s, the flame remains V-shaped and anchors farther downstream. The particular value of $A_s = 1.15 \times 10^{-2}$ is sufficient to suppress all the asymmetric flames of the pure gaseous combustion (Fig. 2a) having inlet velocities as high as 185 cm/s (see Fig. 2e); for $U_{IN} > 185$ cm/s the flames are blown out (Fig. 2e) such that there is only heterogeneous hydrogen conversion.

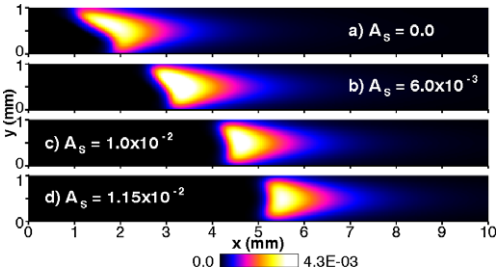

Fig. 3. Iso-contours of OH mass fraction at $U_{IN} = 165$ cm/s for different surface reactivities A_s: (a) pure gas-phase combustion ($A_s = 0.0$); (b) $A_s = 6.0 \times 10^{-3}$; (c) $A_s = 1.0 \times 10^{-2}$; (d) $A_s = 1.15 \times 10^{-2}$.

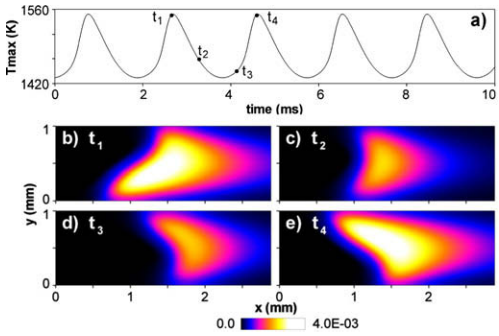

Fig. 4. Oscillating flame at $U_{IN} = 103.5$ cm/s and $A_s = 1.0 \times 10^{-3}$: (a) temporal variation of the maximum temperature; (b)–(e) Y_{OH} iso-contours at the four times t_1 to t_4 marked in (a) ($t_1 = 2.65$ ms, $t_2 = 3.28$ ms, $t_3 = 4.14$ ms, $t_4 = 4.58$ ms).

The oscillating flame, which is a periodic transition between the upper and lower asymmetric flames (exemplified in Fig. 4 by the Y_{OH} distribution at four time intervals of the oscillation period), is even more sensitive to the presence of surface reactions. For the oscillating flame at $U_{IN} = 103.5$ cm/s (a value well-inside the narrow stability range of this flame type), Fig. 5 provides the amplitude ($T_{c,max} - T_{c,min}$) and the frequency of the maximum temperature oscillations inside the channel with increasing A_s; ($T_{c,max} - T_{c,min}$) is the difference between the maximum temperature at the peak of the cycle and the maximum temperature at the dip of the cycle. With rising A_s, the oscillations are still sustained, however, with decreasing amplitude and frequency. When A_s is increased from 3.0×10^{-3} to 4.0×10^{-3} the nature of the flame dynamics changes; the oscillations cease and the flame exhibits a new mode, which we refer to as pulsating: the flame always maintains the same asymmetric shape (either upper or lower) and moves back and forth in the streamwise direction. This flame type remains stable up to $A_s = 5.0 \times 10^{-3}$. With a further increase to $A_s = 6.0 \times 10^{-3}$, the pulsations die out and the asymmetric steady flame is obtained.

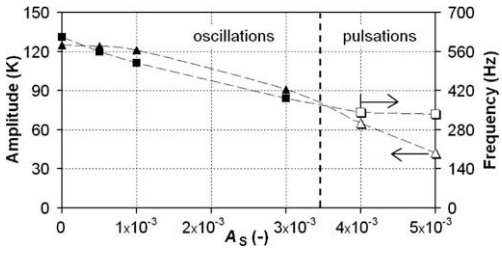

Fig. 5. Oscillating flame at $U_{IN} = 103.5$ cm/s: amplitude ($T_{c,max} - T_{c,min}$) and frequency of temperature oscillations for different values of the surface reactivity A_s. The open squares and triangles refer to pulsating flames.

We have thus identified the minimum values of A_s for which the asymmetric and the oscillating flames are suppressed ($A_s = 1.15 \times 10^{-2}$ and 5.0×10^{-3}, respectively), and also the extreme A_s where pulsating flames first appear ($A_s = 3.0 \times 10^{-3}$) and then disappear ($A_s = 6.0 \times 10^{-3}$).

For the four specific values of the surface reactivity $A_s = 3.0 \times 10^{-3}$, 5.0×10^{-3}, 6.0×10^{-3} and 1.15×10^{-2}, the inflow velocity has been varied systematically so as to cover all possible flame positions within the computational domain. The results are presented in Fig. 2b–e for increasing A_s. At $A_s = 3.0 \times 10^{-3}$ (Fig. 2b), the dynamics have already changed considerably compared to pure homogeneous combustion (Fig. 2a): the ignition/extinction mode has been suppressed, and the pulsating mode has emerged right at the extremes of the stability range of the oscillating flame. In Fig. 6, the iso-contours of the H radical mass fraction (Y_H) are depicted for the different flame types and for $A_s = 3.0 \times 10^{-3}$. At $U_{IN} = 50$ cm/s, the flame is V-shaped (Fig. 6a). When the inlet velocity is increased to 83 cm/s, two maxima (symmetric with respect to the midplane) appear in the Y_H distribution (the maxima of all the other species and of temperature remain on the midplane); at $U_{IN} = 85$ cm/s (Fig. 6c), one of the two Y_H maxima becomes predominant (in this case the lower one, but both lower and upper solutions are equally probable) such that the flame assumes an asymmetric shape; at $U_{IN} = 87$ cm/s the flame starts to pulsate (in a fashion similar to the pulsations of Fig. 6e for $U_{IN} = 108$ cm/s). When the inlet velocity is further increased, oscillating flames appear (Fig. 6d for $U_{IN} = 100$ cm/s). The time evolution of the maximum temperature inside the channel is also plotted in the inset: in addition, Y_H iso-contours, corresponding to the two time instants, t_1 and t_2 shown in the same figure, are also provided. At higher inflow velocities, the flame approaches again the pulsating regime as seen in Fig. 6e for $U_{IN} = 108$ cm/s (Y_H iso-contours at the two time instants marked on the maximum temperature curve are shown, with the solid and dotted lines corresponding to t_1 and t_2, respectively). Finally, for $U_{IN} > 110$ cm/s, the asymmetric flame type appears and remains stable until it is blown out of the domain, Fig. 6f and g.

Increasing A_s to 5.0×10^{-3}, the oscillating flame type is completely suppressed and only the V-shaped, the pulsating, and the asymmetric flames are left (Fig. 2c). At even higher surface reactivity, $A_s = 6.0 \times 10^{-3}$, the pulsating flame is also suppressed (Fig. 2d). Finally, at $A_s = 1.15 \times 10^{-2}$, only the V-shaped flame remains stable over the entire range of U_{IN} (Fig. 2e and Fig. 7).

For all investigated values of the surface reactivity, the repetitive ignition/extinction mode is suppressed. The underlying reason is that at low inlet velocities (small Peclet numbers) of this mode, the heterogeneous pathway is very effective

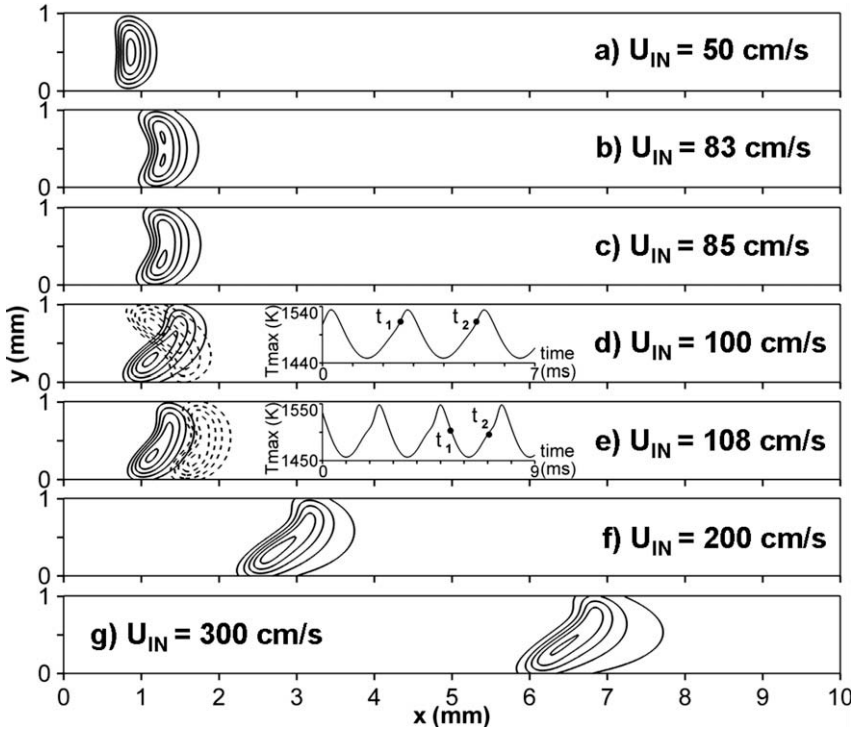

Fig. 6. Flame dynamics for $A_s = 3.0 \times 10^{-3}$. Iso-lines of H mass fraction for: (a) V-shaped flame; (b) V-shaped flame with two Y_H maxima; (c) asymmetric flame; (d) oscillating flame; (e) pulsating flame; (f) and (g) asymmetric flames, for U_{IN} as indicated. In (d) and (e) the temporal variation of the maximum temperature is shown: the Y_H solid-iso-lines refer to the time instants t_1 [$t_1 = 2.57$ ms in (d) and 5.31 ms in (e)] and the dotted-iso-lines to t_2 [$t_2 = 5.06$ ms in (d) and 7.05 ms in (e)]. Five iso-lines ranging from 1×10^{-5} to 1.3×10^{-4}, 2.1×10^{-4}, 2.2×10^{-4}, 6.3×10^{-4}, 3.0×10^{-4}, 4.5×10^{-4}, and 6.6×10^{-4} in (a)–(g), respectively, are plotted.

in consuming the hydrogen, depriving it from the gas-phase and hence inhibiting homogeneous ignition. Thus, at the lowest values of the inflow velocity, only flameless, pure heterogeneous conversion is observed. This new combustion mode, marked in Fig. 2b–e with an open square, is denoted by "no flame". Finally, with increasing surface reactivity, the maximum value of U_{IN} for which flames can be sustained inside the channel is reduced (see Fig. 2e, $U_{IN,max} = 185$ cm/s for $A_s = 1.15 \times 10^{-2}$).

The suppression of all non-stationary flame modes (ignition/extinction, oscillating and pulsating) is desirable as these modes may compromise the reactor performance and integrity. The asymmetric mode is also undesirable: in real systems, the presence of small experimental variations results in temporally random transitions between the "upper" and "lower" flame structures [5]. Therefore, the catalytic activity on the wall provides a very effective method for eliminating all non-stationary combustion modes. Depending on the fuel, catalyst and geometry, an analysis similar to the one outlined previously can provide the minimum catalytic reactivity (A_s) needed to suppress flame dynamics while still maintaining predominantly gas-phase combustion. A catalyst with a predetermined noble-metal loading can be applied at the channel walls so as to reproduce this minimum heterogeneous reactivity. It is stressed that the aforementioned methodology maintains a flame in the reactor, at least for a sub-range of the inlet velocities of the non-catalytic case. For very high catalytic reactivities, gas-phase combustion may be altogether suppressed [28]. Although pure catalytic combustion can be an option for certain devices, the presence of a flame has the added advantage of ensuring complete fuel conversion at short channel lengths,

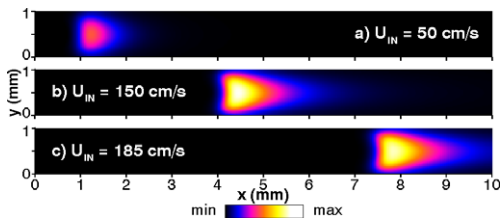

Fig. 7. Flame dynamics for $A_s = 1.15 \times 10^{-2}$. Iso-contours of Y_{OH} ($1.0 \times 10^{-6} \leqslant Y_{OH} \leqslant 3.5 \times 10^{-3}$) for U_{IN} as indicated.

which may have otherwise been impossible due to the mass transport limitations of the catalytic pathway.

3.3. Impact of catalytic reactions on homogeneous ignition

A qualitative analysis is carried out to understand the influence of the catalytic reactivity on the flame stability, as well as the sensitivity of the flame anchoring point to changes in gas-phase reaction parameters. An analytical homogeneous ignition criterion for channel-flow catalytic combustion has been constructed by Mantzaras and Appel [28] using matched activation energy asymptotics. The homogeneous ignition criterion explicitly includes the effects of finite-rate surface and gas-phase chemistry, and reads as:

$$\frac{\zeta_{ig} F(\zeta_{ig})}{\Delta^*_{cr}} = \frac{A}{2Pr}\frac{1}{Da_g}\Omega(Da_s). \quad (3)$$

For the ensuing discussion it is sufficient to note that the left side of Eq. (3) is a monotonically increasing function of the non-dimensional homogeneous ignition distance $\zeta_{ig} = x/(hRe_{IN}\,Pr)$, with x, Re_{IN} and Pr the ignition distance, inlet Reynolds number and the constant Prandtl number, respectively. In the right side of Eq. (3), A is a function of the inlet and wall temperatures, and of the gas-phase exothermicity and reactivity; Da_g is a gas-phase Damköhler number [28] and $\Omega(Da_s)$ is a monotonically increasing function of the surface Damköhler number Da_s:

$$Da_s = hB_s \exp(-E_s/RT_W)/\alpha_{th,IN}, \quad (4)$$

where B_s and E_s are the pre-exponential and activation energy of a global catalytic reaction and $\alpha_{th,IN}$ is the inlet mixture thermal diffusivity. The criterion of Eq. (3) implies that an increase in Da_g or a decrease in Da_s promotes the onset of homogeneous ignition (ζ_{ig} is reduced). Using Eq. (3) we investigate the sensitivity of the homogeneous ignition distance to changes in the gas-phase Damköhler number (e.g. due to fluctuations in the inlet fuel concentration, etc.). The graph of Fig. 8 provides $d\zeta_{ig}/dDa_g$ versus ζ_{ig} for different Da_s. On the same graph, the lines corresponding to $Da_s = 1.5$ and 5.9, correspond to the extreme values of A_s examined in this work (3.0×10^{-3} and 1.15×10^{-2}). These lines were constructed using a global catalytic step for hydrogen oxidation on Pt, of the type presented in Schefer [29], $\dot{s}_{H_2} = B_s \exp(-E_s/RT_W)[H_2]_w$, with $B_s = 6 \times 10^3$ cm/s, $E_s = 14.9$ kJ/mol and $[H_2]_w$ the hydrogen concentration at the wall in mol/cm^3. This step reproduced within 10% the profiles of Fig. 1 (see e.g. the two lines marked with symbols in Fig. 1). The effect of A_s was accounted for in Eq. (4) as a multiplicative factor to B_s.

As clearly seen in Fig. 8, the lower the Da_s, i.e. the lower the surface reactivity, the more sensitive the ignition distance becomes to changes in Da_g. Moreover, this sensitivity diminishes rapidly with increasing Da_s, such that a considerable amount of the change in $d\zeta_{ig}/dDa_g$ occurs in the narrow range $0 \leqslant Da_s \leqslant 5.9$ examined in this study. It is plausible that at these low ranges of Da_s, where the anchoring point of the flame is most sensitive to changes in gas-phase reaction parameters, flame instabilities may occur. It is also plausible to expect that at sufficiently high values of Da_s where this sensitivity diminishes, flame instabilities may be suppressed. Nonetheless, a theoretical stability analysis is needed to rigorously identify the origins of the flame dynamics suppression.

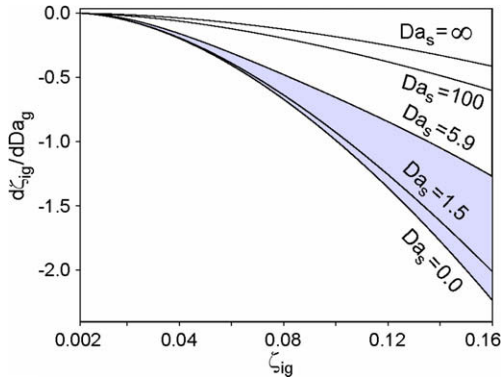

Fig. 8. Sensitivity of the non-dimensional homogeneous ignition distance (ζ_{ig}) to changes in the gas-phase Damköhler number (Da_g): $d\zeta_{ig}/dDa_g$, vs. ζ_{ig}, for different surface Damköhler numbers (Da_s).

4. Conclusions

The dynamics of lean premixed hydrogen/air flames were investigated numerically in a 1-mm-height microchannel as a function of the inlet velocity and the wall catalytic reactivity. The latter was controlled by the parameter A_s, the ratio of the catalytically active to the geometrical surface area. It was shown that the initially rich flame dynamics of the non-catalytic case, which included repetitive ignition/extinction, oscillating and asymmetric flame modes, were suppressed by catalytic reactions. The repetitive/ignition extinction was suppressed at $A_s = 3 \times 10^{-3}$, the oscillating/pulsating flames were eliminated at $A_s = 6 \times 10^{-3}$ and the asymmetric ones at $A_s = 1.15 \times 10^{-2}$, leaving only the stable and symmetric V-shaped combustion mode at higher A_s. The suppression of the flame dynamics can be attributed to the diminishing sensitivity of the homogeneous ignition distance to changes in gas-phase reaction parameters with increasing catalytic reactivity. Finally, the results suggest that a feasible way to eliminate undesirable flame dynamics in microchannels is to apply a predetermined catalyst loading on the channel walls.

The active catalyst loading required to suppress specific flame modes, depends on the particular fuel and catalyst type.

Acknowledgments

Support has been provided by the Swiss National Foundation via contract 200021-109398. AGT acknowledges the support of the Greek Ministry of Development.

Appendix A. Supplementary data

Supplementary data associated with this article can be found, in the online version, at doi: 10.1016/j.proci.2008.05.055.

References

[1] A.C. Fernandez-Pello, *Proc. Combust. Inst.* 29 (2002) 883–899.
[2] J.M. Ahn, C. Eastwood, L. Sitzki, P.D. Ronney, *Proc. Combust. Inst.* 30 (2005) 2463–2472.
[3] D.G. Norton, E.D. Wetzel, D.G. Vlachos, *Ind. Eng. Chem. Res.* 43 (2004) 4833–4840.
[4] S. Karagiannidis, J. Mantzaras, G. Jackson, K. Boulouchos, *Proc. Combust. Inst.* 31 (2007) 3309–3317.
[5] U. Dogwiler, J. Mantzaras, P. Benz, B. Kaeppeli, R. Bombach, A. Arnold, *Proc. Combust. Inst.* 27 (1998) 2275–2282.
[6] K. Maruta, J.K. Parc, K.C. Oh, T. Fujimori, S.S. Minaev, R.V. Fursenko, *Combust. Explos. Shock Waves* 40 (2004) 516–523.
[7] K. Maruta, T. Kataoka, N.I. Kim, S. Minaev, R. Fursenko, *Proc. Combust. Inst.* 30 (2005) 2429–2436.
[8] F. Richecoeur, D.C. Kyritsis, *Proc. Combust. Inst.* 30 (2005) 2419–2427.
[9] G. Pizza, C.E. Frouzakis, J. Mantzaras, A.G. Tomboulides, K. Boulouchos, *Combust. Flame* 152 (2008) 433–450.
[10] J. Vican, B.F. Gajdeczko, F.L. Dryer, D.L. Milius, I.A. Aksay, R.A. Yetter, *Proc. Combust. Inst.* 29 (2002) 909–916.
[11] D. Kyritsis, I. Guerrero-Arias, S. Roychoudhury, A. Gomez, *Proc. Combust. Inst.* 29 (2002) 965–972.
[12] D.G. Norton, D.G. Vlachos, *Proc. Combust. Inst.* 30 (2005) 2473–2480.
[13] K. Maruta, K. Takeda, J. Ahn, K. Borer, L. Sitzki, P.D. Ronney, O. Deutschmann, *Proc. Combust. Inst.* 29 (2002) 957–963.
[14] M. Reinke, J. Mantzaras, R. Bombach, S. Schenker, A. Inauen, *Combust. Flame* 141 (2005) 448–468.
[15] C. Appel, J. Mantzaras, R. Schaeren, R. Bombach, A. Inauen, *Combust. Flame* 140 (2005) 70–92.
[16] M.E. Coltrin, R.J. Kee, F.M. Rupley, *Surface Chemkin: A Fortran Package for Analyzing Heterogeneous Chemical Kinetics at the Solid Surface–Gas Phase Interface*, Report No. SAND90-8003C, Sandia National Laboratories, 1996.
[17] A. Schneider, J. Mantzaras, S. Eriksson, *Combust. Sci. Technol.* 180 (2008) 89–126.
[18] S. Eriksson, A. Schneider, J. Mantzaras, M. Wolf, S. Järås, *Chem. Eng. Sci.* 62 (2007) 3991–4011.
[19] T.J. Kim, R.A. Yetter, F.L. Dryer, *Proc. Combust. Inst.* 25 (1994) 759–766.
[20] O. Deutschmann, R. Schmidt, F. Behrendt, J. Warnatz, *Proc. Combust. Inst.* 26 (1996) 1747–1754.
[21] R.J. Kee, G. Dixon-Lewis, J. Warnatz. M.E. Coltrin, J.A. Miller, *A Fortran Computer Code Package for the Evaluation of Gas-Phase Multicomponent Transport Properties*, Report No. SAND86-8246, Sandia National Laboratories, 1996.
[22] R.J. Kee, F.M. Rupley, J.A. Miller, *Chemkin II: A Fortran Chemical Kinetics Package for the Analysis of Gas-Phase Chemical Kinetics*, Report No. SAND89-8009B, Sandia National Laboratories, 1996.
[23] M.O. Deville, P.F. Fischer, E.H. Mund, *High-Order Methods for Incompressible Fluid Flow*, Cambridge University Press, New York, 2002.
[24] A.G. Tomboulides, J. Lee, S.A. Orszag, *J. Sci. Comp.* 12 (1997) 139–167.
[25] G.D. Byrne, A.C. Hindmarsh, *Int. J. High Perform. Comput. Appl.* 13 (1999) 354–365.
[26] T. Poinsot, D. Veynante, *Theoretical and Numerical Combustion*, Edwards, Philadelphia, 2005, 56 pp.
[27] F.M. Rupley, R.J. Kee, J.A. Miller, *Premix: A Fortran Program for Modeling Steady Laminar One-Dimensional Premixed Flames*, Report No. SAND85-8240, Sandia National Laboratories, 1995.
[28] J. Mantzaras, C. Appel, *Combust. Flame* 130 (2002) 336–351.
[29] R.W. Schefer, *Combust. Flame* 45 (1982) 171–190.